www.czasopisma.pan.pl PAN www.journals.pan.pl

Metrol. Meas. Syst., Vol. XXII (2015), No. 3, pp. 429–442.

PAN POLSKA AKADEMIA NAUK

METROLOGY AND MEASUREMENT SYSTEMS

Index 330930, ISSN 0860-8229

www.metrology.pg.gda.pl

M&MS

AN UNCERTAINTY MODEL OF APPROXIMATING THE ANALYTICAL SOLUTION TO THE REAL CASE IN THE FIELD OF STRESS PREDICTION

Ramón Gutiérrez, María Ramírez, Ester Olmeda,Vicente Díaz

Universidad Carlos III de Madrid, Mechanical Engineering Department, Leganés, Avda. de la Universidad, 3028911, Leganés, Madrid, Spain (✉ ragutier@ing.uc3m.es, +34 916 249 905, mrami@ing.uc3m.es, eolmeda@ing.uc3m.es, vdiaz@ing.uc3m.es)

Abstract

Deterministic mechanics has been extensively used by engineers as they needed models that could predict the behavior of designed structures and components. However, modern engineering is now shifting to a new approach where the uncertainty analysis of the model inputs enables to obtain more accurate results. This paper presents an application of this new approach in the field of the stress analysis. In this case, a two-dimensional stress elasticity model is compared with the experimental stress results of five different size tubes measured with resistive strain gages. Theoretical and experimental uncertainties have been calculated by means of the Monte Carlo method and a weighted least square algorithm, respectively. The paper proposes that the analytical engineering models have to integrate an uncertainty component considering the uncertainties of the input data and phenomena observed during the test, that are difficult to adapt in the analytical model. The prediction will be thus improved, the theoretical result being much closer to the real case.

Keywords: uncertainty, strain gage measurement, stress concentration factor, weighted least square algorithm.

© 2015 Polish Academy of Sciences. All rights reserved

1. Introduction

Deterministic structural mechanics has been extensively used by mechanical engineers as they needed models that could predict the behavior of designed structures and components [1]. From the metrological approach, it has to be assumed that theoretical models are based on principles that can never be met in a real case since the behaviour of input variables feeding the model, as element geometry, material properties and applied loads, is also of stochastic nature. Thus, it can be inferred that approximation of the model to reality can be then quantified in terms of bias and uncertainty.

The level of compliance of a model with a given real case is fully quantified only if both experimental and model results are presented with their correspondent uncertainty [2]. Nevertheless, the criteria of tolerance for its acceptance have to be decided by the engineers according to the accuracy required in their work field, depending on the conflict between structural integrity and cost optimization [3].

At the same time, important engineering decisions in industry are based in computational solid mechanics without their credibility being really quantified. Engineering associations and research centers [2, 4–6] offer guides for a better understanding of numerical model validation metrics.

From the point of view of uncertainty quantification, analytical models are much easier to assess whether using the law of propagation of uncertainties or the practical alternative of Monte Carlo Method (MMC) [7].

According to the metrology criteria of the GUM [8], the error is understood as a result of the measurement minus a conventional true value of the measurand because the true value itself cannot be determined. In this case, the measurand, or the particular quantity subject to

Article history: received on Feb. 18, 2015; accepted on Apr. 30, 2015; available online on Sep. 21, 2015; DOI: 10.1515/mms-2015-0031.

measurement, is defined as the tangential stress measured in five different size tubes compressed by two flat surfaces. The comparison of the results can be made by means of calculating the difference between the average magnitudes. However, the comparative analysis will not be complete if the incidence of uncertainties in both results is not assessed, as it has to be understood that uncertainty provides a range of possible values where the measurand can be found [8].

The reviewed literature evidences that the publication of practical cases in the field of stress model validation where the uncertainty is taken into account is scarce. This paper presents a real case of how a controlled stress experiment with a profusely used strain gage technique can produce a new approach to comparison of the experimental and theoretical results, considering also uncertainty of the last ones.

In this paper, the general elasticity expression developed by Chianese and Erdlac [9] is used and compared with the experimental results. The benefit of using strain gages is that it will be possible to know the evolution of the tangential stress σ_P with respect to the applied force; hence it will be feasible to calculate the stress concentration factor by the resultant slope between σ_P and $4P/\pi LD$.

This is possible using a weighted least square algorithm [10] that considers the randomness of the variance of both Cartesian axes, so the average stress concentration factor and its uncertainty can be found. Furthermore, an adaptive Monte Carlo procedure for calculating the theoretical model uncertainty is implemented [7].

2. Analytical model

The two-dimensional analytical solution of the circular ring with a concentric hole and rectangular cross section (Fig. 1) is obtained by the superposition of two stress states [11]. The first state considers the stresses in a disk compressed by two equal and opposite forces, and the second accounts for a ring, where the stress in its inner rim cancels the stress in the disk of the same value of radius r' [12].

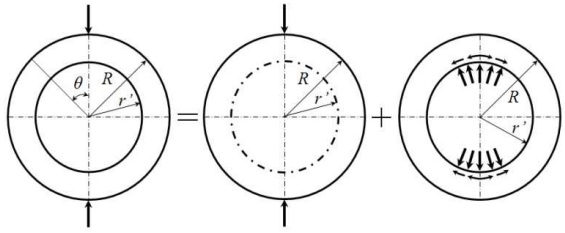

Fig. 1. Superposition of the stress in the compressed ring.

The procedure to find the exact solution of this two-dimensional problem was first discussed by Timoshenko [13] and has been developed by Chianese and Erdlac [9] for any relationship between the radii and valid for any point of the ring. Other solutions were developed by authors like Nelson [14], Ripperger [15] and Batista [16] producing nearly identical results.

When the tangential stress distribution in a ring is studied, the stress concentration factor K concept is normally used [13], as it is a dimensionless magnitude that depends exclusively on the radii ratio ρ and the angle θ where the stress is calculated. Therefore rings with different size but with the same ρ present the identical value of K.

Since the objective of this paper is to compare the experimental stress concentration factor in the outer surfaces of the tubes (K_E) with the corresponding theoretical solution, only the

Metrol. Meas. Syst., Vol. XXII (2015), No. 3, pp. 429–442.

analytical solution of the tangential stress $\sigma_{\theta\theta}$ of a ring compressed by two opposite forces is needed. So, the theoretical stress developed by Chianese and Erdlac [9] is expressed:

$$\sigma_{\theta\theta} = \frac{2P}{\pi l R} K = \frac{4P}{\pi l D} K, \tag{1}$$

where the stress concentration factor K for the tangential stress in any given point of the ring is:

$$K = \frac{1}{2} - \frac{1\rho^2}{2r^2}\left(\frac{1+r^2}{1-\rho^2}\right) - \frac{(1-r\cos\theta)\sin^2\theta}{(r^2+1-2r\cos\theta)^2} - \frac{(1+r\cos\theta)\sin^2\theta}{(r^2+1+2r\cos\theta)^2} + \sum_{n=2}^{\infty}\Big[n(n-1)\,c_n r^{n-2} + \\ + (n+2)(n+1)d_n r^n + n(n+1)c_n' r^{-n-2} + (n-2)(n-1)d_n' r^{-n}\Big]\cos n\theta \tag{2}$$

and the coefficients are defined as:

$$c_n = \frac{1}{2(n-1)D}\left[n(\rho^2-1) + (\rho^{2n}-1) - n^2\left(\rho - \frac{1}{\rho}\right)^2\right],$$

$$d_n = \frac{1}{2(n+1)D}\left[n^2\left(\rho - \frac{1}{\rho}\right)^2 + n\left(\frac{1}{\rho^2}-1\right) - (\rho^{2n}-1)\right],$$

$$c_n' = \frac{1}{2(n+1)D}\left[n(\rho^2-1) + (\rho^{2n}-1)\right],$$

$$d_n' = \frac{1}{2(n-1)D}\left[n\left(\rho - \frac{1}{\rho}\right)^2 + (\rho^{2n}-1)\right],$$

$$D = n^2\left(\rho - \frac{1}{\rho}\right)^2 - \left(\rho^n - \frac{1}{\rho^n}\right)^2.$$

Up to this date, the theoretical results developed by the authors cited before have been compared with their corresponding experimental results, by means of photo-elasticity [14]. It was demonstrated that in a hollow cylinder the stress distribution along the length is quite uniform, so the problem could be treated as a two-dimensional one [14]. Their results produced differences between the model and experiment, ranging from 0.2% to 3.64%. Nevertheless, the uncertainty of the experiment and the model was not considered for the model validation.

The two-dimensional model can thus be extrapolated to a three-dimensional state, considering that the tube is composed by infinite summation of rings of the same stress. However, it is known that real tubes do not strictly fulfill this condition as they present a higher stress in the proximity of their borders, so the stress distribution is therefore not constant. The stress behavior of real and finite tubes can then be approximated to the two-dimensional model, but with certain limits.

3. Methodology

In order to quantify the aforementioned problem, five seamless alloy-steel tubes E-355 of different diameters and thicknesses were used (Table 1). To ensure uniformity of the diameters along their lengths and their concentricity, turning the outside diameter and boring the inside

diameter was done in one set-up, that is, without moving the work-piece between both operations. The applied load was such, that in none of the cases the yield strength value of the tested material was exceeded.

Table 1. Tube dimensions and applied compression loads.

Tube	Outer diameter D (mm)	Inner diameter d (mm)	Length L (mm)	$\rho = d/D$ (mm/mm)	Compression Load P (kN)	Young Modulus E (Pa)
1	75.73	60.10	99.25	0.793	27.93	2.176×10^{11}
2	98.47	82.30	87.68	0.836	20.11	2.063×10^{11}
3	125.68	107.55	79.98	0.856	18.00	2.119×10^{11}
4	149.60	132.80	80.08	0.888	12.96	2.130×10^{11}
5	233.49	205.60	80.50	0.881	24.19	2.066×10^{11}

The five tubes were instrumented along their lengths with four tee rosettes; model FCA-6-11 with the following disposition. Rosette #1 was located as close as possible to the tube border; rosette #2 was in the middle of the tube and rosette #3 was located at the middle distance between rosettes 1 and 2. In order to control the symmetry of the applied load, one additional strain gage rosette was fixed in the middle of the length of the opposite side. The distributions of the strain gage rosettes are shown in Fig 2a. For all the strain gages a three-wire quarter Wheatstone bridge circuit was employed [17].

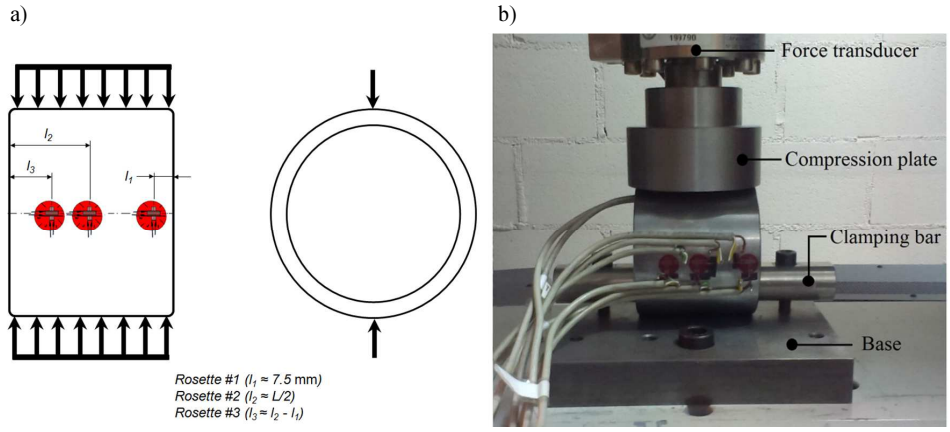

Fig. 2. Distribution of the strain gage rosettes in the compressed tube: a) schematic representation; b) experimental mounting.

3.1. Experimental data processing

The tubes have been tested using a compression testing machine installed in a controlled climate room (23°C). For the load application, a compression plate and a base were especially manufactured and installed to the force transducer and the machine test bench, respectively. The tube was fixed to the base to protect against it moving (Fig. 2b).

The force P and the strain data were recorded at the 10 Hz frequency; the force was increased at the rate of 50 N until its maximum value was reached (Table 1). The obtained force and strain data was exported in ASCII format to be analyzed later by a numerical computing program. Fig. 3 shows the flowchart for estimation of the experimental stress concentration factor K_E. This procedure was repeated 10 times for each tube.

Metrol. Meas. Syst., Vol. XXII (2015), No. 3, pp. 429–442.

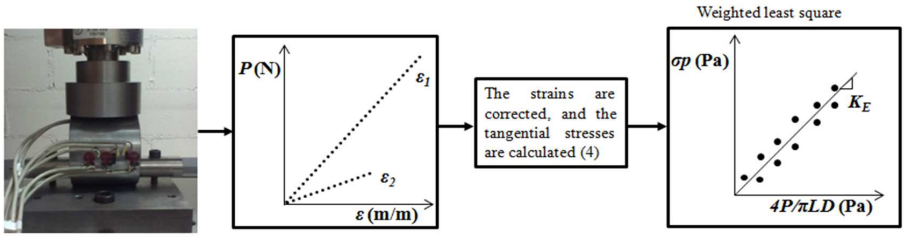

Fig. 3. The flowchart for estimation of the experimental stress concentration factor K.

The strain total error has to be calculated taking into account all sources of the error [18–22]. As the principal strain directions are known, it is possible to consider that the misalignment error is produced by the gap existing between the gage axes and the principal strain axes. Therefore, it was only necessary to transform the strain reading previously corrected to the principal axes of the strain by a Mohr's circle, as seen in (3), [21]:

$$\varepsilon_{P,Q} = \frac{\varepsilon_1 + \varepsilon_2}{2} \pm \frac{\varepsilon_1 - \varepsilon_2}{2\cos(2\beta)}, \tag{3}$$

where ε_1 and ε_2 are the corrected strain gage readings from the axes x and y that are misaligned by the angle β from the directions of the minimum and maximum strains ε_Q and ε_P, respectively.

For calculation of the experimental principal stress σ_P, we assume that the test material is homogeneous and isotropic in its mechanical properties. So, the biaxial form of Hooke's law can be used to convert the principal strains (3) into the principal stresses [21]. The tangential stress is then calculated by the following equation:

$$\sigma_P = \frac{E}{1-\nu^2}\left(\varepsilon_P + \nu\varepsilon_Q\right), \tag{4}$$

where E is the Young Modulus and ν is the Poisson ratio.

Afterwards, the tangential stress σ_P was plotted versus the ratio $4P/\pi LD$ and a linear relationship was observed. Therefore, the slope that represents the experimental stress concentration factor, K_E, has been calculated using a weighted least square algorithm [10].

3.2. Determination of the experimental stress concentration factor and its uncertainty

In this paper, the Williamson-York method [10] is used to estimate the experimental stress concentration factor K_E. The Williamson-York method is a weighted least square algorithm for calculating the best straight line when the variances in both axes exist – in our case $u^2(\sigma_P)$ and $u^2(4P/\pi LD)$ – thus allowing to reach an acceptable value [23].

To estimate the uncertainty of the experimental stress concentration factor K_E using strain gages, it is necessary to evaluate the uncertainty caused by different sources of error, because K_E is not measured directly. The experimental stress concentration factor represents the slope between the tangential stress σ_P and the ratio $4P/\pi LD$. Therefore, it is necessary to apply the law of propagation of uncertainty to calculate the variances of the y axis (σ_P) and the x axis ($4P/\pi LD$) [24].

3.2.1. Uncertainty of the y axis

The combined standard uncertainty of the corrected strain (ε_1 and ε_2) was calculated with (5), according to the expression developed by Montero *et al*. (Table 2) [24]:

$$u_c(\varepsilon_i) = \sqrt{u^2(\hat{\varepsilon}_i) + u^2(E_{W,i}) + u^2(E_{T,i}) + u^2(E_{TS,i})}. \tag{5}$$

Table 2. Variance of the strain measurement.

Variance due to	Formula
The strain measuring instrument	$u(\hat{\varepsilon}_i) = \frac{a}{\sqrt{3}}$ a = 0.5 με
Wheatstone bridge nonlinearity	$u^2(E_{w,i}) = \left[\frac{\partial E_{w,i}}{\partial \hat{\varepsilon}_i} u(\hat{\varepsilon}_i)\right]^2 + \left[\frac{\partial E_{w,i}}{\partial F} u(F)\right]^2$ $\hat{\varepsilon}_i$: the strain indicated by the strain data acquisition system; F : the gage factor.
Temperature	$u^2(E_{T,i}) = \left[\frac{\partial E_{T,i}}{\partial F} u(F)\right]^2 + \left[\frac{\partial E_{T,i}}{\partial \alpha_G} u(\alpha_G)\right]^2 + \left[\frac{\partial E_{T,i}}{\partial T_E} u(T_E)\right]^2 + \left[\frac{\partial E_{T,i}}{\partial T_c} u(T_c)\right]^2 +$ $+ \left[\frac{\partial E_{T,i}}{\partial \varepsilon_{T/0}} u(\varepsilon_{T/0})\right]^2 + \left[\frac{\partial E_{T,i}}{\partial \alpha_{s(B)}} u(\alpha_{s(B)})\right]^2 + \left[\frac{\partial E_{T,i}}{\partial \alpha_{s(A)}} u(\alpha_{s(A)})\right]^2$ α_G : the temperature coefficient of the gage factor; T_E , T_C : the temperatures of the test piece and the roomtemperature on the gage package data label, respectively; $\varepsilon_{T/0}$: the thermal output or apparent strain; $\alpha_{s(B)}$: the coefficient of thermal expansion of the test material; $\alpha_{s(A)}$: the coefficient of thermal expansion of the material used by the strain gage manufacturer.
Transverse sensitivity	$u^2(E_{TS,i}) = \left[\frac{\partial E_{TS,i}}{\partial \nu_0} u(\nu_0)\right]^2 + \left[\frac{\partial E_{TS,i}}{\partial K_t} u(K_t)\right]^2 + \left[\left\lvert\frac{\partial E_{TS,i}}{\partial \hat{\varepsilon}_x} u(\hat{\varepsilon}_x)\right\rvert + \left\lvert\frac{\partial E_{TS,i}}{\partial \hat{\varepsilon}_y} u(\hat{\varepsilon}_y)\right\rvert\right]^2$ $\hat{\varepsilon}_x$, $\hat{\varepsilon}_y$: the uncorrected strain of gages 1 and 2 of the tee rosette; K_t : the transverse sensitivity coefficient; ν_0 = 0.285

Once the variance for each of the components forming (5) is calculated, it is possible to obtain the combined variances of the principal strains (6):

$$u^2(\varepsilon_{P,Q}) = \left[\frac{\partial \varepsilon_{P,Q}}{\partial \beta} u(\beta)\right]^2 + \left[\frac{\partial \varepsilon_{P,Q}}{\partial \varepsilon_1} u(\varepsilon_1)\right]^2 + \left[\frac{\partial \varepsilon_{P,Q}}{\partial \varepsilon_2} u(\varepsilon_2)\right]^2. \tag{6}$$

As the magnitudes E and ν have been obtained by simultaneous observations, a correlation between them exists [8]. Therefore, the combined variance of the tangential stress is:

$$u^2(\sigma_P) = \left[\frac{\partial \sigma_P}{\partial \varepsilon_P} u(\varepsilon_P)\right]^2 + \left[\frac{\partial \sigma_P}{\partial \varepsilon_Q} u(\varepsilon_Q)\right]^2 + \left[\frac{\partial \sigma_P}{\partial E} u(E)\right]^2 + \left[\frac{\partial \sigma_P}{\partial \nu} u(\nu)\right]^{\wedge 2} + \tag{7}$$
$$+ 2\frac{\partial \sigma_P}{\partial E}\frac{\partial \sigma_P}{\partial \nu} u(E,\nu),$$

where: $u(E,\nu) = \frac{1}{n(n-1)} \sum_{i=1}^{n} (E_i - E)(\nu_i - \nu)$.

Metrol. Meas. Syst., Vol. XXII (2015), No. 3, pp. 429–442.

3.2.2. Uncertainty of the x axis

The uncertainty of the x axis is influenced by the force data acquisition system and the instrument used to characterize geometrically the tubes. By applying the law of propagation of uncertainty to this term and considering the correlation between L and D [25], as they were measured with the same caliper, the expression of the x axis combined variance could be calculated as follows:

$$u^2(x) = \left[\frac{\partial x}{\partial P}u(P)\right]^2 + \left[\left|\frac{\partial x}{\partial l}u(L)\right| + \left|\frac{\partial x}{\partial D}u(D)\right|\right]^2. \tag{8}$$

3.2.3. Uncertainties of the experimental stress concentration factor

The experimental stress concentration factor K_E and its uncertainty $u(K_E)$ for each repetition i has been calculated using the weighted least squares algorithm [10], as it allows to obtain estimates of standard errors which are correct under arbitrary heteroskedasticity [26]. Moreover, the final value of the experimental stress concentration factor is the mean of n observations (n = 10*)* made, *i.e.*:

$$\bar{K}_E = \frac{1}{n}\sum_{i=1}^{n} K_{E,i}. \tag{9}$$

So, the standard uncertainty associated with $\bar{K}_E$ (12) considers contribution of the uncertainty of each observation (10), and the experimental standard deviation of $\bar{K}_E$ (11).

$$u(K_E) = \frac{1}{n}\sum_{i=1}^{n} u(K_{E,i}), \tag{10}$$

$$s^2(\bar{K}_E) = \frac{\sum_{i=1}^{n}(K_{E,i} - \bar{K}_E)^2}{n(n-1)}. \tag{11}$$

Therefore:

$$u(\bar{K}_E) = \sqrt{u^2(K_E) + s^2(\bar{K}_E)}. \tag{12}$$

The expanded uncertainty (13) is calculated according to annex G of GUM [8] and computing the effective degrees of freedom v_{eff} from the Welch-Satterthwaite equation. Thus, the coverage factor k = 2 is determined for an approximate level of confidence of 95 %.

$$U(\bar{K}_E) = 2u(\bar{K}_E). \tag{13}$$

As the experimental stress concentration factor is averaged along the tube length, and because the theoretical model assumes a uniform distribution which we want to verify, the uncertainty due to this average has to be taken into account. Considering that all the possible values of the experimental stress concentration factor are between the calculated maximum and minimum, the uncertainty can be estimated with (14):

$$u(\bar{K}_{E,av}) = \frac{\bar{K}_{E,\max} - \bar{K}_{E,\min}}{\sqrt{12}}. \tag{14}$$

Table 3 summarizes all the variables used to calculate the experimental stress concentration factor K_E and its uncertainties. Several uncertainties were calculated by means of type B evaluation, assuming a symmetric rectangular distribution.

The Young's modulus E and Poisson ratios v have been calculated from flat specimens taken from the tubes [27]. The tests were performed as recommended by ASTM [28, 29]. Note, that some of the variables have been presented in the following form: *e.g.* E_i is the Young's modulus, where i represents the number of the tube where the variable was measured.

Table 3. Values and uncertainty of all the variables.

Variable	Value	Units	Tolerance	Semi-range *a*	Uncertainty *u*
F	2.10	Dimensionless	$\pm 1.00\times10^{-2}$	1.00×10^{-2}	5.77×10^{-3}
K_t	1.00×10^{-3}	Dimensionless	-1.00×10^{-3}	1.00×10^{-3}	5.77×10^{-4}
α_G	1.00×10^{-2}	°C^{-1}	$\pm 5.00\times10^{-5}$	5.00×10^{-5}	2.89×10^{-5}
v_0	0.285	Dimensionless	$\pm 1.00\times10^{-2}$	1.00×10^{-2}	5.77×10^{-3}
β	$-1.05\times10^{-2} \leq \beta \leq 1.75\times10^{-2}$	Radians	$\pm 8.73\times10^{-4}$	–	9.60×10^{-4}
L D	See Table 1	mm	$\pm 1.00\times10^{-1}$	–	2.15×10^{-2}
d	See Table 1	mm	$\pm 5.00\times10^{-1}$	–	2.89×10^{-2}
$T_{E,1}$	21	°C	±1.00	1.00	5.77×10^{-1}
$T_{E,2}$	21				
$T_{E,3}$	23				
$T_{E,4}$	25				
$T_{E,5}$	21				
$\varepsilon_{T/0,1}$	3.80×10^{-1}	µm/m	–	–	8.50×10^{-1} (µm/m)/°C
$\varepsilon_{T/0,2}$	3.80×10^{-1}				
$\varepsilon_{T/0,3}$	8.96×10^{-1}				
$\varepsilon_{T/0,4}$	1.09				
$\varepsilon_{T/0,5}$	3.80×10^{-1}				
P	Varies	kN	–	–	$2.5\times10^{-3}P$
T_C	23	°C	–	–	–
$\alpha_{s(A)}$	11.8×10^{-6}	°C^{-1}	–	–	–
$\alpha_{s(B)}$	11.7×10^{-6}	°C^{-1}	–	–	–
Values and uncertainty of the test material using type A evaluation					
E_1	2.176×10^{11}	Pa	–	–	1.95×10^{9}
E_2	2.063×10^{11}		–	–	6.14×10^{8}
E_3	2.119×10^{11}		–	–	1.79×10^{8}
E_4	2.130×10^{11}		–	–	4.77×10^{8}
E_5	2.066×10^{11}		–	–	1.79×10^{8}
v_1	3.010×10^{-1}	Dimensionless	–	–	2.03×10^{-4}
v_2	3.000×10^{-1}		–	–	2.00×10^{-4}
v_3	3.043×10^{-1}		–	–	2.05×10^{-4}
v_4	2.909×10^{-1}		–	–	2.98×10^{-4}
v_5	2.893×10^{-1}		–	–	1.11×10^{-4}

3.3. Uncertainty of the theoretical stress concentration factor

The expression of Theory of Elasticity (2) is rather complex to be derived; therefore, application of the law of propagation of uncertainty according to GUM JCGM [8] is quite tedious. For these cases, the JCGM has implemented the Monte Carlo Method, as it is possible to generate a population of random data for each input variable once its upper and lower limits

Metrol. Meas. Syst., Vol. XXII (2015), No. 3, pp. 429–442.

are known, and then to estimate the standard deviation of the theoretical stress concentration factor K from the values returned by the random input data [7].

An adaptive Monte Carlo procedure [7] is used for the uncertainty of K, because the theoretical expression is given as an infinite summation. Therefore, the adaptive procedure allows us to do in a few minutes a calculation that could take several hours.

The adaptive procedure is based on carrying out an increasing number of Monte Carlo trials expressed by h until the magnitudes that are equal to twice the standard deviation of the stress concentration factor; its uncertainty and its upper and lower limits $(2s_K, 2s_{u(K)}, 2s_{K_L}, 2s_{K_H})$ are less than the numerical tolerance associated with the uncertainty $u(K_{MC})$, in this case $\delta = 1/2.10^l$ [7]. The inputs of the theoretical stress concentration factor are D, d and θ. As their uncertainties are known (Table 3), the Gaussian probability distribution function was selected. Therefore, according to GUM [7], the coverage factor of 2 is used, corresponding to the coverage probability of approximately 95%.

3.4. Theoretical model enhancement by means of uncertainty

The variations of the experimental concentration factor along the tube length are due to real effects that are not considered in the two-dimensional and ideal theoretical model. However, the designer needs a model for his stress predictions that allows him to calculate the possible stress limits in order to confront them with the design specifications. In this context, the uncertainty analysis and quantification offers a possibility to enhance the two-dimensional model, so that it can take into account the real three-dimensional effects.

As proposed in this paper, it is obtained by incrementing the uncertainty calculated for the elasticity model $u\left(K_{MC}\right)$ with the experimental uncertainty generated by the distribution of the stress concentration factor along the tube length, $u\left(\bar{K}_{E,av}\right)$. The standard uncertainty associated to the model will be then:

$$u\left(K\right) = \sqrt{u^2\left(K_{MC}\right) + u^2\left(\bar{K}_{E,av}\right)}. \tag{15}$$

With this approach we are not changing the results predicted by the model, but we improve the possible results associated to the prediction, when the assumption of uniform stress along the length is not possible.

4. Results and discussion

The maximum error in strain measurements due to several sources [18–22] was < 1 $\mu\varepsilon$, that represents 0.1% of the maximum strain recorded. Even though the error values have remained relatively low, they were not discarded, *i.e.*, all the recorded strains have been corrected in order to obtain the highest possible accuracy in calculation of the experimental stress concentration factor $\bar{K}_E$.

The differences between the experimental stress concentration factor $\bar{K}_E$ calculated from the readings of the gages on opposite sides of the tubes were not significant (< 0.5%). This ensures that the distribution of the stresses due to the alignment of the load has been symmetrical in all the tubes tested.

On the other hand, the distribution of the stress concentration factor along the tube length presents a higher uniformity between gages when the length vs diameter (L/D) ratio increases. The variation of the results is below 1% except for tube 5, where the measurement of the gage closer to the edge increases this variation up to 2.24%. This can be caused by the fact that as

the L/D ratio decreases, the tube resembles less the ideal case, so the border effect produces a higher and negative influence on the uniformity of stress distribution. Table 4 shows the values of uncertainties calculated in point 3.2.3 for the five tested tubes. It can be seen that – in the majority of cases – the uncertainty due to the weighted least square has a greater impact than the one calculated by repeatability. This demonstrates that the constant experimental conditions throughout the tests ensure the quality of results. Moreover, the uncertainty due to variation along the length $u\left(\overline{K}_{E,av}\right)$ has the highest weight of all and is caused by the negative influence of the border effect explained above, which is shown in Fig. 4.

Table 4. Uncertainty of the experimental stress concentration factor $\overline{K}_E$.

Tube	Weighted least square	Experimental standard deviation of the mean	Uncertainty of $\overline{K}_E$	Average along the length
	Equation (10)	Equation (11)	Equation (12)	Equation (14)
1	0.15	0.05	0.15	0.22
2	0.12	0.00	0.12	0.45
3	0.17	0.02	0.17	0.80
4	0.18	0.12	0.22	1.02
5	0.06	0.31	0.32	2.26

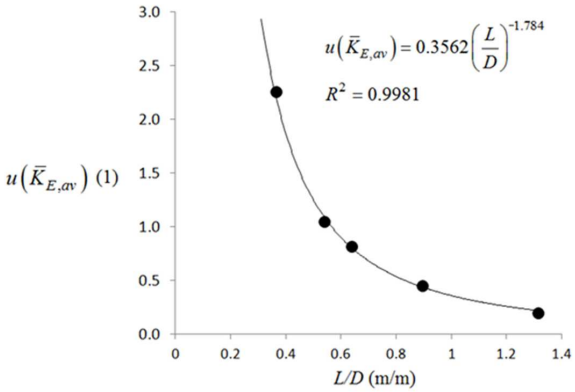

Fig. 4. Evolution of $u\left(\overline{K}_{E,av}\right)$ with the L/D ratio.

Figure 4 shows the values of $u\left(\overline{K}_{E,av}\right)$ for each tube, represented by the L/D ratio. As it can be seen, evolution of this uncertainty can be expressed by an exponential function of the L/D ratio with the regression factor $R^2 = 0.9981$. Fig. 4 also demonstrates that for $L/D > 1.2$ the magnitude of $u\left(\overline{K}_{E,av}\right)$ reaches values of the same order than the other components of uncertainty. When the tube is of infinite length its contribution will be nearly zero, this evolution being consistent with the principles of the elasticity model.

Integration of this uncertainty component in the uncertainty attributed to the theoretical model (15) will enhance its accuracy, as it will provide the designer with more realistic limits to its design which, from the engineering point of view, is based on its probability of failure.

As for the influence of the variables considered in the theoretical model, it has been observed that $u\left(K_{MC}\right)$ increases as the radii ratio ρ also increases. The minimum value is found for tube 1: $u\left(K_{MC}\right) = 0.15$, and the maximum – for tube 4: $u\left(K_{MC}\right) = 0.47$. Taking into account the

Metrol. Meas. Syst., Vol. XXII (2015), No. 3, pp. 429–442.

uncertainties of the model variables (*D, d, L* and *θ*) and the uncertainty due to the experimental variation of $\bar{K}_E$ along the tube length, $u\left(\bar{K}_{E,av}\right)$, the stress model would present higher uncertainty for a thin wall tube with a big diameter compared to its length.

Table 5 shows the mean experimental stress concentration factor $\bar{K}_E$ for the five tubes and the respective theoretical values of *K* calculated with (2).

Table 5. The final results of the experimental stress concentration factor, theoretical values, error and experimental uncertainty for the confidence level of 95%.

	Tube 1 (ρ = 0.793)	**Tube 2 (ρ = 0.836)**	**Tube 3 (ρ = 0.856)**	**Tube 4 (ρ = 0.888)**	**Tube 5 (ρ = 0.881)**
$\bar{K}_E$	30.61	52.13	66.18	116.01	104.33
$U\left(\bar{K}_E\right)$	0.31	0.24	0.34	0.43	0.63
K	29.97	50.75	67.79	116.98	102.25
U(K)	0.53	1.00	1.69	2.25	4.56
$Error = K - \bar{K}_E$	–0.64	–1.38	1.61	0.97	–2.08
$\%Error = 100\dfrac{Error}{K}$	–2.13	–2.72	2.37	0.83	–2.03

The relative differences between the experimental and theoretical results vary from 0.83% for tube 4 to –2.72% for tube 2. From the quantitative point of view it can be inferred that the differences are small and coincident with the ranges found by other authors [14]. Moreover, having controlled other influencing parameters, as the temperature, the differences are not showing any particular tendency, so it can be assumed that they are due to uncontrolled phenomena and/or the difference between the ideal two-dimensional model and real specimen.

As for the uncertainties, the theoretical *U*(*K*) is always higher than the experimental one and – in the case of tube 5 – even seven times higher due to the already mentioned border effect.

Figure 5 shows the significance of introducing the uncertainty $u\left(\bar{K}_{E,av}\right)$ due mainly to the border effect. Following the indication of Sandia [4], the global uncertainty, that is the joined theoretical and experimental uncertainties, is repreresented around the theoretical result and is calculated with the following equation:

$$U\left(K_{global}\right) = 2\sqrt{u^2\left(K\right) + u^2\left(\bar{K}_E\right)}. \tag{16}$$

This allows to clearly check if the experimental result is within the range of possible values given by the global uncertainty, and to avoid false positives when the ranges $U(K)$ and $U\left(\bar{K}_E\right)$ have a certain level of coincidence – without meaning that the model prediction agrees with the experimental result.

As it can be seen in Fig. 5, if $u\left(\bar{K}_{E,av}\right)$ is taken into account, the experimental results are clearly within 95% confidence bounds for four of the five tubes. This indicates that the model predictions are consitent with the experimental results. If $u\left(\bar{K}_{E,av}\right)$ is not considered this only happens for tube 4. From the point of view of safe design, the engineer can then trust that the stress model prediction generates a range of possible values where the experimental value is included. The exponential regression calculated for $u\left(\bar{K}_{E,av}\right)$ in Fig. 4 is thus very useful, as it provides the engineer with a tool to quantify how close or far is the ideal model from the real case he has to work with. Up to this moment, it was generally assumed that the two-dimensional

model could be used for long tubes, but this term did not correspond to any specific L/D ratio. Moreover, the model uncertainty considered for other tube dimensions had not yet been quantified. It is then up to the engineer to decide on the level of uncertainty he can require from the model depending on the aplication field.

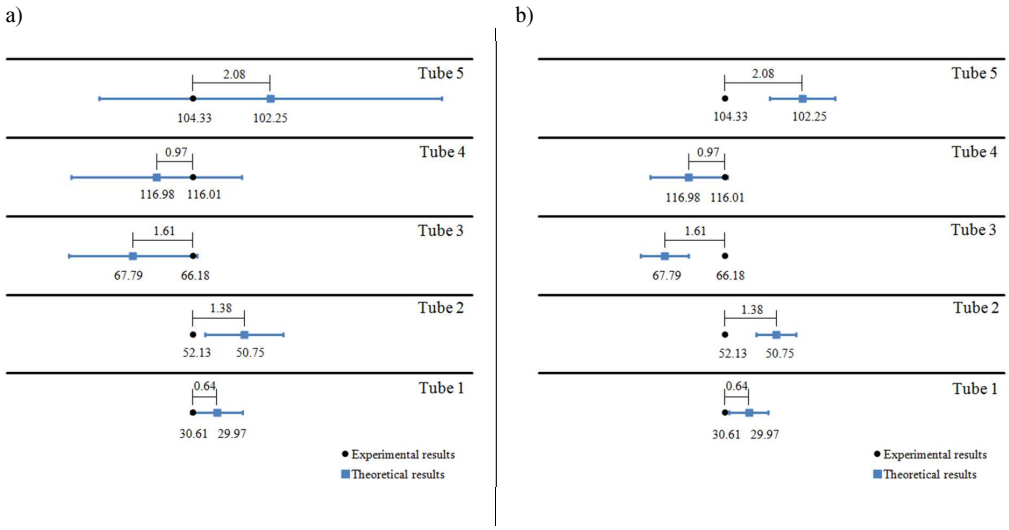

Fig. 5. Differences between the experimental and theoretical results for each of the tubes tested including their uncertainty for the 95% level of confidence: a) with $u\left(\overline{K}_{E,av}\right)$; b) without $u\left(\overline{K}_{E,av}\right)$.

5. Conclusions

Up to this moment, many authors [1, 3, 30] have proposed a new methodology for model validation considering the uncertainty range in both theoretical and experimental data. This produces a deeper knowledge of influence of the variables involved both in the model and in the real phenomenon. This paper presents a real case of this new approach in the field of stress mechanics. A numerical example is given for the circumferential stress in the outer surface of a tube, compressed by two symmetric forces acting along its diameter, by means of an experiment using the strain gage, in terms of the stress concentration factor K.

The results show a good agreement of experimental and theoretical models for what is usually expected in the engineering field. It can be seen that the differences between them are always below 3% and their uncertainties are under 1% and 4.5% of their average values, respectively.

The results presented in this paper quantify influence of the design parameter on the uncertainties of experiments, but also on the model. Moreover, it is proposed to increase the model uncertainty with its component due to the stress variation along the length caused by the border effect, $u\left(\overline{K}_{E,av}\right)$. It has been demonstrated that this inclusion improves the prediction of the model, as it increases the range of possible values, being thus better adapted to the situation where a tube does not meet the ideal infinite length condition. This practical case shows then an example on how powerful tool can be metrology for engineers, not only for validation of models, but also providing a better knowledge of the parameters that have a greater influence on both the model and the experiment. The designer is thus aware of the aspects that can be improved to minimize the difference between model and experiments or the limits he cannot surpass in using the model according to the design criteria.

The proposed methodology has been developed for steel tubes, as it is the most common material used in machine design. Nevertheless, it should be confirmed in further research with other materials.

References

[1] Elishakoff, I. (2013). Recent developments in applied mechanics with uncertainties. *4th Inverse problems, design and optimization symposium.*

[2] Liu, Y., Chen, W., Arendt, P., Huang, H. (2011). Toward a better understanding of model validation metrics. *J. Mech. Des.*, 133(7), 071005–1–13.

[3] Sebastian, C., Hack, E., Patterson, E.A. (2012). An approach to the validation of computational solid mechanics models for strain analysis. *J. Strain Anal. Eng.,* 48(1), 36–47.

[4] Hills, R.G., Trucano, T.G. (1999). *Statistical validation of engineering and scientific models: Background.* Sandia National Laboratories, Report No. SAND99–1256.

[5] Schwer, L.E. (2007). An Overview of the PTC 60/V&V 10: Guide for verification and validation in computational solid mechanics. *Eng. Comput.*, 23(4), 245–252.

[6] Thacker, B.H., Doebling, S.W., Hemez, F.M., Anderson, M.C., Pepin, J.E., Rodriguez, E.A. (2004). *Concepts of model verification and validation*. Los Alamos National Laboratory, LA–14167–MS.

[7] BIPM, IEC, IFCC, ILAC, ISO, IUPAC, IUPAP, OIML (2008). JCGM 101: Evaluation of measurement data – Supplement 1 to the Guide to the expression of uncertainty in measurement – Propagation of distributions using a Monte Carlo method.

[8] BIPM, IEC, IFCC, ILAC, ISO, IUPAC, IUPAP, OIML (2008). JCGM 100: Evaluation of measurement data – Guide to the expression of the uncertainty in measurement.

[9] Chianese, R.B., Erdlac, R.J. (1988). The general solution to the distribution of stresses in a circular ring compressed by two forces acting along a diameter. *Q. J. Mechanics Appl. Math.*, 41(2), 239–247.

[10] Williamson, J.H. (1968). Least-squares fitting of a straight line. *Can. J. Phys.*, 46, 1845–1847.

[11] Timoshenko, S.P. (1922). On the distribution of stresses in a circular ring compressed by two forces acting along a diameter. *Philos. Mag.*, 44, 1014–1019.

[12] Timoshenko, S.P. (1951). *Theory of Elasticity.* United States: McGraw-Hill.

[13] Timoshenko, S.P. (1910). Stresses in a circular ring compressed by two opposing forces. *Proc. Kiev Polytech. Inst.*, 9, 21–37.

[14] Nelson, C.W. (1939). *Stresses and Displacements in a Hollow Circular Cylinder.* Ph.D. Thesis. University of Michigan.

[15] Ripperger, E.A., Davids, N. (1947). Critical stresses in a circular ring. *Proc. ASCE*, 112(1), 619–628.

[16] Batista, M., Usenik, J. (1996). Stresses in a circular ring under two forces acting along a diameter. *J. Strain Anal. Eng.*, 31(1), 75–78.

[17] Vishay Micro-Measurements (2010). The three-wire quarter-bridge circuit. *Application note TT–612*, 221–223.

[18] Vishay Micro-Measurements (2010). Errors due to Wheatstone bridge nonlinearity. *Technical note TN–507–1*, 77–81.

[19] Vishay Micro-Measurements (2010). Strain gage thermal output and gage factor variation with temperature. *Technical note TN–504–1*, 35–47.

[20] Vishay Micro-Measurements (2010). Errors due to transverse sensitivity in strain gages. *Technical note TN–509*, 91–99.

[21] Vishay Micro-Measurements (2008). Strain gage rosettes: Selection, application and data reduction. *Technical note TN–515*, 151–161.

[22] Vishay Micro-Measurements. (2010). Errors due to misalignment of strain gages. *Technical note TN–511*, 107–111.

[23] Cantrell, C.A. (2008). Technical Note: Review of methods for linear least–squares fitting of data and application to atmospheric chemistry problems. *Atmos. Chem. Phys.*, 8, 5477–5487.

[24] Montero, W., Farag, R., Díaz, V., Ramirez, M., Boada, B. (2011). Uncertainties associated with strain–measuring systems using resistance strain gauges. *J. Strain Anal. Eng.*, 46(1), 1–13.

[25] EA Laboratory Committee (2013). *EA–4/02 M: 2013 Evaluation of the uncertainty of measurement in calibration*.

[26] Brown, L.C., Berthouex, P.M. (2002). *Statistics for Environmental Engineers*. United State: Lewis Publishers.

[27] ASTM International (2008). ASTM E8M–04 Standard test methods for tension testing of metallic materials [Metric], West Conshohocken, PA.

[28] ASTM International (2004). ASTM E111–04 Standard test method for Young's modulus, tangent modulus, and chord modulus, West Conshohocken, PA.

[29] ASTM International (2010). ASTM E132–04 Standard test method for Poisson's ratio at room temperature, West Conshohocken, PA.

[30] Elishakoff, I., Ohsaki, M. (2010). *Optimization and Anti–Optimization of Structures Under Uncertainty*. London: Imperial College Press.